RSC Advances

PAPER

View Article Online
View Journal | View Issue

Cite this: *RSC Adv.*, 2017, **7**, 10407

Reductive removal of gaseous nitrous oxide by activated carbon with metal oxide catalysts

Hong Meng,[b] Linpo Yuan,[ab] Jiajun Gao,[c] Nannan Ren,[b] Yingzhou Lu[b] and Chunxi Li*[ab]

Received 18th November 2016
Accepted 2nd February 2017

DOI: 10.1039/c6ra26983d

rsc.li/rsc-advances

The efficient reductive decomposition of gaseous nitrous oxide (N_2O) from industrial effluents is of practical importance in abating greenhouse gas emissions. In the present study, active carbon (AC) has been chosen as both a reductive agent and a catalyst support. Dozens of AC-based catalysts with different kinds and amounts of metal oxide have been prepared under various conditions and characterized. The performances of Cu-containing AC have been studied at varying gas flow rates, Cu contents, and calcination temperatures. N_2O in a gas mixture (42% N_2O, 58% N_2) was found to be completely removed by Cu-loaded AC (9 wt% Cu, calcined at 400 °C) at 325 °C with a GHSV of 2293 h^{-1}. This process is viable by virtue of the low cost of AC and easier manipulation and process control in comparison with alternative methods employing reductive gases such as hydrogen and ammonia.

1. Introduction

Nitrous oxide (N_2O) is a greenhouse gas with a global warming potential value of about 310. As a by-product of the manufacture of several chemical products, such as adipic acid and nitric acid, its atmospheric concentration has increased significantly over the last decades, and continues to increase by 0.2–0.3% per year.[1] This inexorable trend has attracted a great deal of attention for the development of an efficient method for the removal of N_2O from industrial exhausts, especially for the tail gas of the adipic acid production process using HNO_3 as oxidizing agent, where the N_2O content is as high as 38% along with N_2 48.1%, O_2 4.4%, CO_2 9.5%, and NO 0.03% (in wt%).[2]

A direct decomposition process is generally used for gas effluents with low N_2O concentrations,[3] which operates at high temperatures (>500 °C) with various catalysts, *e.g.*, hydrotalcite-like materials,[4] metal-containing zeolites,[5–7] or supported metal oxides,[8–11] *e.g.* CaO–Co_3O_4,[12] and $NiLaO_x$.[13] The decomposition of N_2O is composed of three steps, *viz.*, adsorption, cleavage of the N–O bond, and desorption of O_2, of which the desorption of O_2 is considered as the rate-limiting step. To promote O_2 desorption, some reductive substances, *e.g.*, CH_4, NH_3,[14] H_2,[15] and CO,[16] have been used to instantly consume the *in situ* generated O_2. However, these reductive gases are expensive and/or explosive, and their flow rate needs dynamic control according to the composition of the gas stream, which complicates the process. Activated carbon (AC), as an inexpensive and active solid reducing agent, can overcome these drawbacks, and is thus worthy of study for the reductive removal of N_2O. In fact, coal char is effective in reducing N_2O and NO to N_2 at combustion temperature,[17] and AC loaded with alkali metal oxides shows better performance. Both Na and K can catalyze the reaction between carbon and N_2O, and K is better than Na.[18,19] The reaction between N_2O and C may also be catalyzed by Ni and Pt, and further promoted by K, as reported by Gonçalves *et al.*[20,21]

To date, little research has been conducted to compare the performances of different metal oxides supported on AC for the removal of N_2O under otherwise identical conditions. In this paper we are focused on the treatment of the tail gas of adipic acid production process through catalytic reduction of N_2O using AC as a solid reducing agent. For this purpose, we made a comparative study on the catalytic performances of different metal oxides for the reduction of N_2O on AC, and CuO is found to be the most efficient one. Based on catalyst characterization, a structure–activity relationship has been elucidated, and a reaction mechanism is proposed.

2. Experimental

2.1 Chemical materials

The AC used was a commercial coconut-shell-derived carbon (Tangshan Hua Neng Technology Carbon Co., Ltd., Tangshan, China). All metal nitrates, *i.e.* $Cu(NO_3)_2\cdot 3H_2O$, $Ce(NO_3)_3\cdot 6H_2O$, $Ni(NO_3)_2\cdot 6H_2O$, $Zn(NO_3)_2\cdot 6H_2O$, $Co(NO_3)_2\cdot 6H_2O$, $Fe(NO_3)_3\cdot 9H_2O$, and $Mn(NO_3)_2$, were of analytical reagent grade (Beijing Chem. Co., Ltd., Beijing, China, purity ≥ 99.0%) and were used as received. All aqueous solutions were prepared with deionized water.

[a]State Key Laboratory of Chemical Resource Engineering, Beijing University of Chemical Technology, Beijing 100029, P. R. China. E-mail: licx@mail.buct.edu.cn; Fax: +86 10 64410308; Tel: +86 10 64410308

[b]College of Chemical Engineering, Beijing University of Chemical Technology, Beijing 100029, P. R. China

[c]School of Chemical Engineering and Pharmacy, Wuhan Institute of Technology, Wuhan 430205, P. R. China

2.2 Pre-treatment of AC

The AC was firstly ground into particles of 10–20 mesh, boiled with deionized water for 15 min, and then washed five times with deionized water. The resultant particles were placed in an oven and dried at 110 °C for 24 h.

2.3 Preparation of AC-supported metal oxide catalysts

Certain amounts (0.1–11 wt%, mass fraction of metal atom in AC) of metal nitrate were weighed and dissolved in water (300 mL), AC (30 g) was added to each metal nitrate solution, and the mixtures were stirred magnetically for 24 h at room temperature. They were then placed in an oven and dried at 90 °C for 72 h until the water had completely evaporated. The resultant AC was transferred to a muffle furnace and calcined at 200, 300, or 400 °C for 2 h. Hereinafter, the obtained catalysts are designated as *x*M-AC-*T*, where M represents the supported metal, *x* is the mass fraction of metal atoms in the AC, and *T* is the calcination temperature.

2.4 Catalyst characterization

Fourier-transform infrared (FTIR) spectra in the range $\nu = 4000$–400 cm^{-1} were recorded at room temperature on a Nicolet 6700 spectrometer. Spectra were collected after 32 scans at 4 cm^{-1} resolution. The spectra were acquired from KBr pellets composed of 1 mg of the samples and 100 mg of KBr dried at 200 °C for 24 h. X-ray diffraction (XRD) patterns of the calcined samples were recorded at room temperature on a D/Max 2500 (VB2+ PC) diffractometer using Cu-K_α radiation, operated at 40 kV and 200 mA. The patterns were recorded over a 2θ range of 10–90° with a 0.02° step size. Simultaneous thermogravimetric analysis (TGA) and derivative thermogravimetric analysis curves were recorded on a TGA/DSC1/1100 SF apparatus at a heating rate of 10 °C min^{-1} over the range 25–700 °C in air. X-ray photoelectron spectroscopy (XPS) spectra were recorded on an ESCALAB 250 apparatus with a scanning electron spectroscopy for chemical analysis (ESCA) microscope equipped with an Al monochromatic X-ray source (300 W), employing a beam diameter of 2 mm in CAE analyzer mode. All binding energies were referenced to the C 1s peak at 285 eV. The individual components were obtained by curve fitting.

2.5 N_2O removal experiments

A stainless steel tubular reactor of Φ_5 (i.d.) × 650 mm (effective length 200 mm) was used to investigate the activity of metal oxides supported on AC for N_2O removal at atmospheric pressure. Catalyst (2.0 g) was loaded into the reactor each time, and the gas mixture (42% N_2O, 58% N_2) was fed at rates varying from 50 to 150 mL min^{-1} by means of a V10FA mass flow controller. The reaction temperature was controlled through a proportion integral derivative (PID)-regulated oven. To compare the catalytic performances of different transition metal oxides, the reaction temperature was varied from 300 to 550 °C in steps of 50 °C. To study the effect of the Cu-loading on the performance of the AC-supported Cu catalysts, the reaction temperature was varied from 300 to 550 °C in steps of 25 °C. Furthermore, the reaction temperature was varied from 150 to 325 °C in steps of 25 °C to evaluate the activities of the catalysts calcined at different temperatures. In all of the experiments, temperature was increased at a rate of 5 °C min^{-1}. At any given temperature, the reaction duration was 1 h. The concentration of N_2O in the outlet gas was monitored online by means of a TM GC7700 gas chromatograph equipped with a TCD and a Porapak Q (6 m × 3 mm) column.

3. Results and discussion

3.1 Characterization of the catalysts

Structural characteristics of AC. The AC support used here is a coconut-shell-derived carbon material, which is commercially available. Its structure has been characterized by many researchers[22–24] using N_2 adsorption–desorption method, and the structural parameters were determined as follows, *i.e.* BET specific area 797 ± 45 m^2 g^{-1}, pore size 2.03 ± 0.07 nm, and total pore volume 0.402 ± 0.02 m^3 g^{-1}. Obviously, the AC has a larger pore volume and specific area with rich porosity and micropores, which is much higher than that of coal chars and comparable with many commercial AC sorbents.[25–27] The pore size and surface area is known to be instrumental for the mass transfer and reactivity for a heterogeneous reaction, and a higher surface area and porosity is helpful for enhancing the dispersion of the catalysts and accessibility of the AC and thus the reduction rate of N_2O. In short, higher surface area favors the catalytic reactivity of N_2O reduction on AC.

FTIR characterization. FTIR spectra of the pristine AC and metal-oxide-loaded AC samples are shown in Fig. 1. All samples showed an absorption at $\nu \approx 3435$ cm^{-1}, which could be ascribed to the stretching vibration of O–H[28,29] due to the presence of water. The water contents of all samples were similar, except for AC-supported $Cu(NO_3)_2$, as evidenced by the similar intensities of their O–H peaks. Furthermore, all of the samples showed two bands centered at $\nu = 2921$ and 2852 cm^{-1} due to asymmetric and symmetric C–H stretching vibrations in aliphatic CH, CH_2, and CH_3 groups.[29,30] A scissor vibration of a CH_2 group is responsible for an absorption peak at $\nu = 1455$ cm^{-1}, which was no longer seen for the metal-oxide-loaded AC samples. For AC-supported $Cu(NO_3)_2$, two bands were seen at $\nu = 1383$ and 1340 cm^{-1} attributable to nitrate ($\nu = 1410$–1340 cm^{-1}),[30] which disappeared in the calcined ACs. From the above results, we can deduce that: (1) all nitrates were decomposed to the corresponding metal oxides upon calcination at 400 °C; (2) the structural change of AC is virtually irrelevant to the metal species.

Fig. 2 shows the FTIR spectra of Cu-loaded AC samples calcined at 200, 300, and 400 °C, respectively. It is evident that the loaded $Cu(NO_3)_2$ was completely converted to CuO in all of the calcined samples.

XRD characterization. The XRD patterns of the pristine and metal-oxide-loaded AC samples are shown in Fig. 3. The pristine AC showed two broad peaks, *viz.* at $2\theta \approx 23°$ and 43°, respectively, which are characteristic of amorphous carbon.[31] These two peaks were also present in the patterns of all of the metal-oxide-loaded AC samples, indicating retention of the amorphous structure of AC in the modified AC catalysts. The pattern for

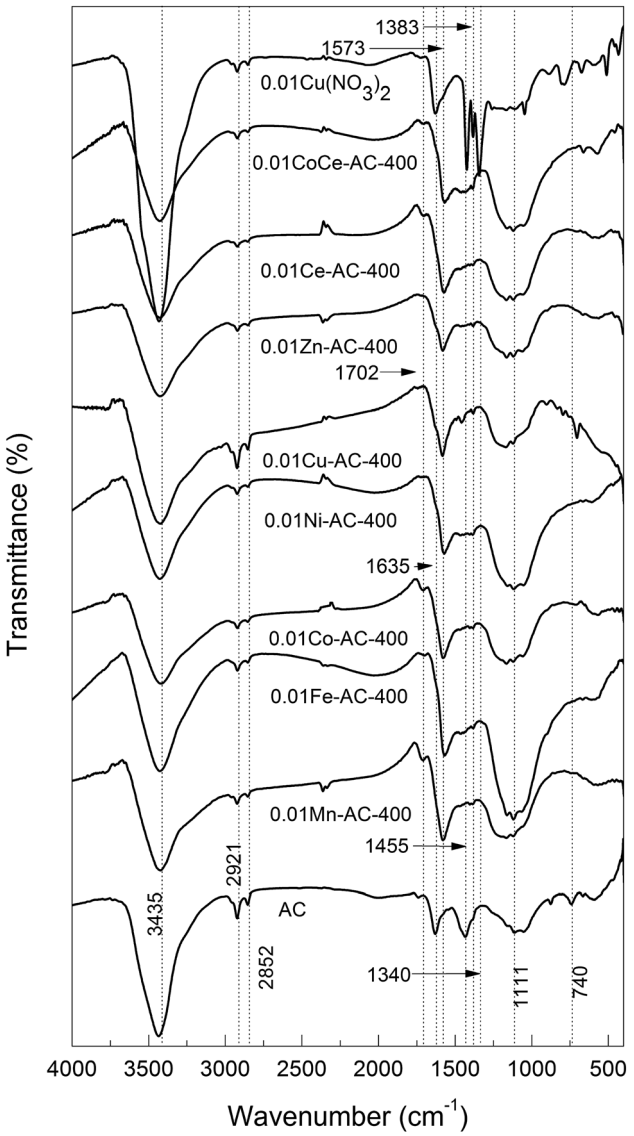

Fig. 1 FTIR spectra of pristine AC and metal-oxide-loaded samples.

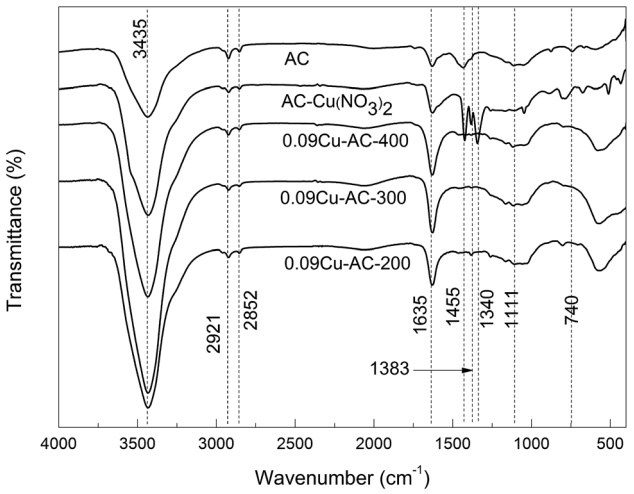

Fig. 2 FTIR spectra of AC with CuO calcined at different temperatures.

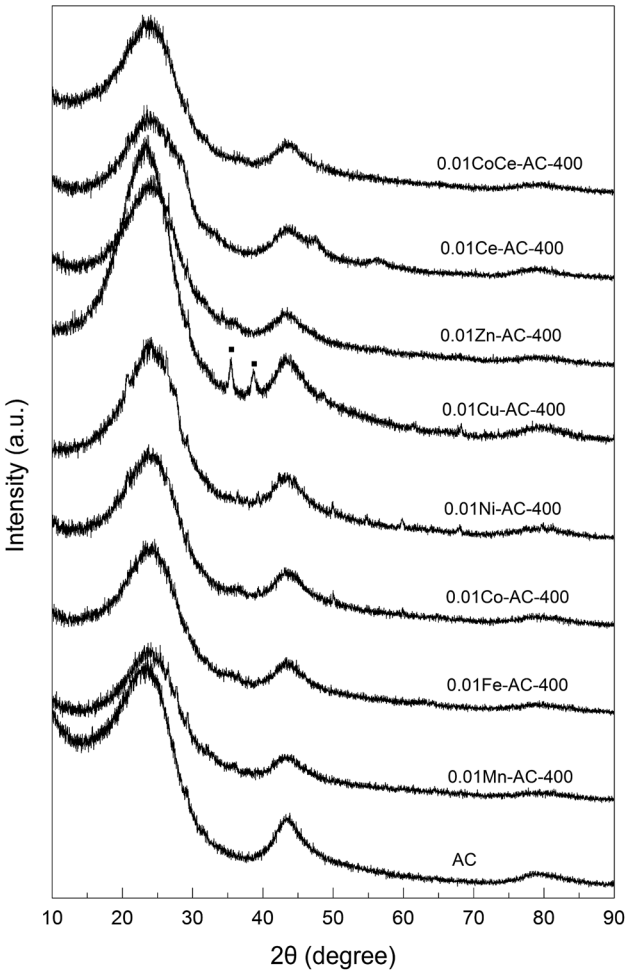

Fig. 3 XRD patterns of pristine AC and metal-oxide-loaded samples.

0.01Cu-AC-400 features two distinct peaks at 35° and 38°, which can be ascribed to CuO (JCPDS).[32] Except for 0.01Cu-AC-400, the diffraction peaks of other metal oxides on the AC samples were virtually unobservable. This may indicate amorphous structures of these metal oxides due to their poor crystallinity at a calcination temperature of 400 °C. Chmielarz *et al.* studied cobalt-containing hydrotalcite-like materials, and found that an amorphous structure of the metal oxide was formed when the calcination temperature was 600 °C, but that the crystallinity increased significantly with temperature.[33] Therefore, the poor crystallinity of some of the present metal oxides on AC may have resulted from the lower calcination temperature.

XRD patterns of the Cu-loaded AC samples calcined at 200, 300, and 400 °C are presented in Fig. 4. Several peaks attributable to CuO and Cu_2O were observed,[32,34] and the intensities of these peaks increased steadily with increasing calcination temperature, implying increasing crystallinity of the copper oxides. Additionally, the content of Cu_2O increased with increasing calcination temperature, suggesting that a certain amount of CuO was reduced by AC at 400 °C.

Thermal analysis. TGA results pertaining to three 0.09Cu-AC samples calcined at 200, 300, and 400 °C are presented in Fig. 5. It can be seen that each of the samples showed a small

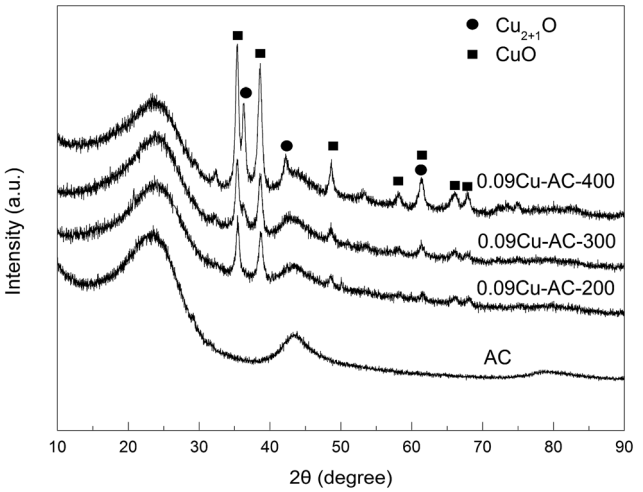

Fig. 4 XRD patterns of AC-supported CuO calcined at different temperatures ($Cu_{2+1}O$ is a crystal mixture of CuO and Cu_2O).

peak before 100 °C due to the evaporation of water. Based on the derivative weight curves, the initiating temperatures of carbon oxidation by air are about 280, 335, and 375 °C for 0.09Cu-AC-200, 0.09Cu-AC-300, and 0.09Cu-AC-400, respectively, and the corresponding temperatures for complete carbon oxidation are about 522, 587, and 607 °C. The reactivity of the metal-oxide-loaded carbon samples decreases with increasing calcination temperature for the Cu-loaded AC catalysts, which may be attributed to the decreasing accessibility of carbon to oxygen due to the blanketing effect of the well-developed metal oxide crystalline layer on the surface of the AC. The results also indicate that AC can also be oxidized by the coexistent O_2 in the gas stream at about 375 °C, indicating that the coexistent O_2 may impose a negative influence on the reduction of N_2O, as discussed latter.

3.2 Comparison of catalytic activities of different metal oxides

The catalytic activities of different metal oxides were evaluated in the tubular reactor using 2 g of each catalyst at a gas flow rate of 100 mL min^{-1}, and the results are shown in Table 1. It can be seen that N_2O was not decomposed over the pristine AC below 350 °C, but its decomposition increased significantly with increasing temperature. For example, the conversion of N_2O increased drastically from 6% at 400 °C to 100% at 550 °C. Moreover, different metal oxides exhibited different activities for the conversion of N_2O. Specifically, 0.01Cu-AC-400 and 0.01Ni-AC-400 completely removed N_2O at 400 °C and 450 °C, respectively. The products were exclusively N_2 and CO_2, as befits the occurrence of the redox reaction between AC and N_2O according to eqn (1):

$$2N_2O + C = 2N_2 + CO_2 \quad (1)$$

As evidenced by the FTIR and XRD results, the major difference between the catalysts lay in the loaded metal species, while the structure of the AC remained essentially the same. Therefore, the reactivity differences of the catalysts can be mainly attributed

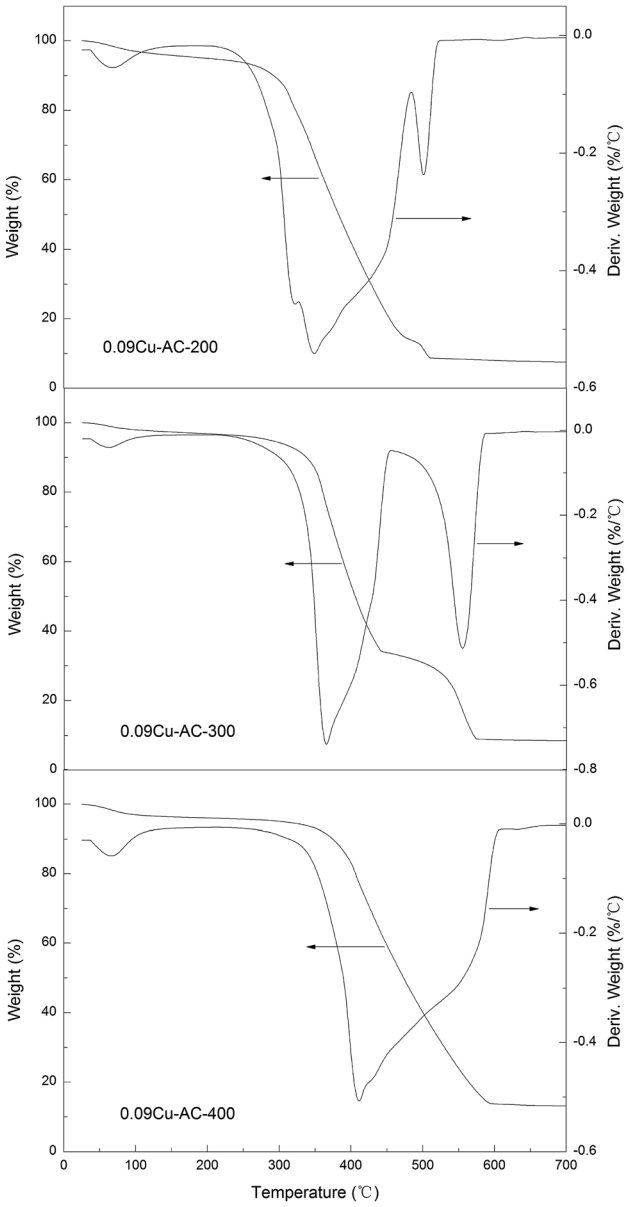

Fig. 5 TGA curves of AC-supported CuO calcined at 200 °C, 300 °C, and 400 °C.

to the different activities of the supported metal oxides for the redox reaction of AC and N_2O. The catalytic activities decreased in the order Cu > Co > Ni > Fe > Mn > Ce > Zn. This order conforms to that reported by Campa *et al.* for the reductive removal of N_2O with CH_4, where the order was Cu > Co > Mn.[35] Therefore, 0.01Cu-AC-400 proved to be the most active catalyst for N_2O removal among all those studied, and was deemed worthy of further study.

3.3 Reactivity of Cu-based ACs under varying conditions

Effect of Cu loading on the catalytic activity. As shown in Fig. 6, the Cu loading had a significant impact on the removal of N_2O. The complete decomposition temperature of N_2O decreased greatly with increasing Cu loading, *e.g.*, from 450 °C to 325 °C as the Cu loading was increased from 0.1 wt% to 9

Table 1 Dependence of conversion of N_2O on temperature

	N_2O conversion (%)					
Pristine/metal-loaded ACs	300 °C	350 °C	400 °C	450 °C	500 °C	550 °C
AC	0	0	6	16	39	100
0.01Mn-AC-400	2	3	13	49	100	—
0.01Fe-AC-400	1	2	17	81	94	100
0.01Co-AC-400	3	13	35	66	100	—
0.01Ni-AC-400	3	5	29	100	—	—
0.01Cu-AC-400	4	18	100	—	—	—
0.01Zn-AC-400	0	1	5	28	100	—
0.01Ce-AC-400	3	4	8	30	100	—
0.01CoCe-AC-400	4	17	35	61	100	—

wt%. At any given temperature, *e.g.* 300 °C, the conversion increased with increasing Cu loading up to 9 wt%, beyond which the Cu loading had little further influence on the activity. Therefore, the optimal Cu loading was determined as 9 wt%.

Effect of calcination temperature. Three Cu-loaded AC samples with different calcination temperatures (200, 300, and 400 °C) were prepared, namely 0.09Cu-AC-200, 0.09Cu-AC-300, and 0.09Cu-AC-400, and their catalytic performances are compared in Fig. 7. Evidently, the calcination temperature had a significant effect on the catalytic reduction of N_2O, and a higher calcination temperature was unfavorable for the catalytic reaction of AC and N_2O. Specifically, the complete removal temperature of N_2O increased steadily from 275 °C for 0.09Cu-AC-200, to 300 °C for 0.09Cu-AC-300, and to 325 °C for 0.09Cu-AC-400. This phenomenon has also been observed by Chmielarz *et al.*,[33] who ascribed it to the changing crystal form and the decreasing surface area with increasing calcination temperature. This explanation is consistent with the increasing crystallinity of copper oxides for 0.09Cu-AC-200, 0.09Cu-AC-300, and 0.09Cu-AC-400, as evidenced by the XRD patterns in Fig. 4.

Effect of gas flow rate. The influence of gas flow on the N_2O removal efficiency was studied for 0.09Cu-AC-400 at three different flow rates, namely 50, 100, and 150 mL min^{-1}, corresponding to GHSV (gas hourly space velocity; ratio of flow rate of N_2O and effective volume of reactor) values of 764.4, 1528.8, and 2293.2 h^{-1}. The results are plotted in Fig. 8. At a lower reaction temperature of 300 °C, the conversion rate of N_2O decreased with increasing gas flow rate, being restricted by the reaction kinetics. The conversion rates of N_2O at the above flow rates were 22%, 21%, and 12%, respectively. However, when the temperature was increased to 325 °C, the conversion rate of N_2O surged to 100% at gas flow rates of 100 and 150 mL min^{-1}, but the N_2O conversion was only 51% at a gas flow rate of 50 mL min^{-1}. This phenomenon could be attributed to the exothermic nature of the reaction and the fast reaction kinetics at a higher temperature. As the flow rate of N_2O is increased, more reaction heat is released due to the efficient oxidation of carbon by N_2O, which raises the temperature of the AC, and thereby accelerates the reaction dramatically. On the other hand, increasing gas flow rate can shorten the retention time, and thus result in incomplete reduction of N_2O. Therefore, the reaction temperature and retention time synergistically determine the effect of flow rate on N_2O conversion. The appropriate GHSV was identified as 2293.2 h^{-1}.

3.4 Catalytic mechanism

The decomposition process of N_2O is believed to involve its redox reaction with carbon under catalysis by the loaded metal

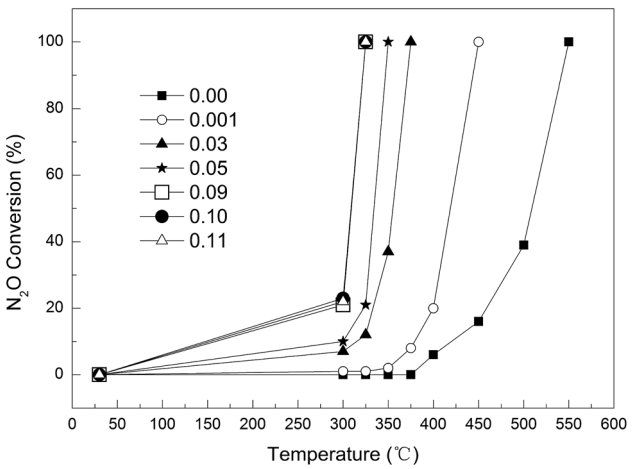

Fig. 6 Effect of Cu loading on N_2O conversion.

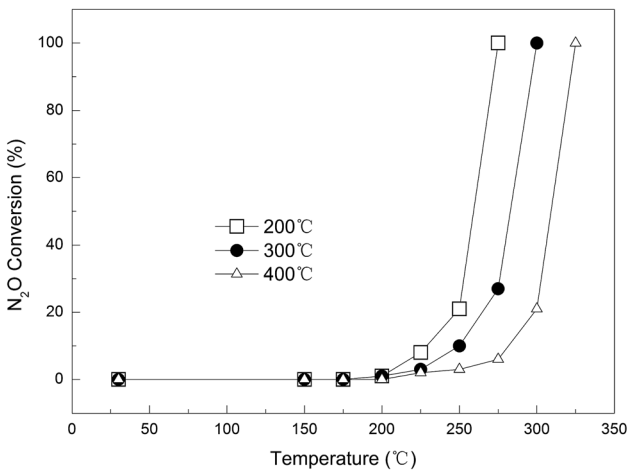

Fig. 7 Dependence of N_2O conversion on calcination temperature.

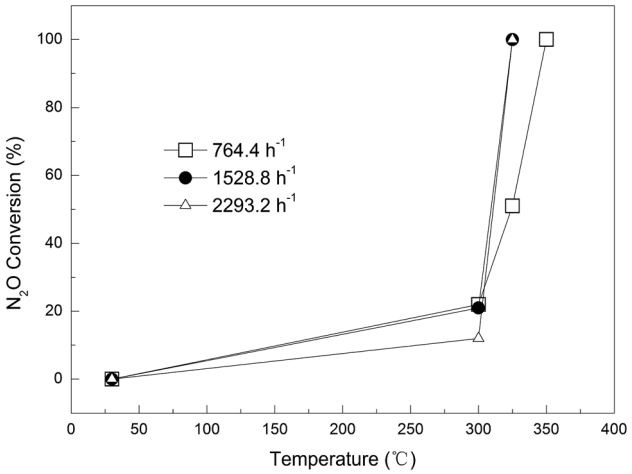

Fig. 8 Effect of gas flow rate on N_2O conversion.

oxide, as is manifested by the consumption of AC and the presence of CO_2 in the gas effluent. However, this process may be achieved in two different ways, *i.e.*, catalytic decomposition of N_2O, forming O_2 and *in situ* oxidation therewith of the carbon support, or reduction of copper oxides by carbon to Cu metal, followed by the *in situ* oxidation of Cu by N_2O. To identify the reaction mechanism, we studied the XPS patterns of three different reagents, namely, the original reactant (OR, 0.03Cu-AC-200), the nitrogen-treated reactant (NTR, obtained by heating OR at 400 °C in N_2 for 5 h), and the used reactant (UR, obtained by heating the NTR at 400 °C in N_2O for 2 h). Fig. 9 shows the Cu 2p XPS spectra.

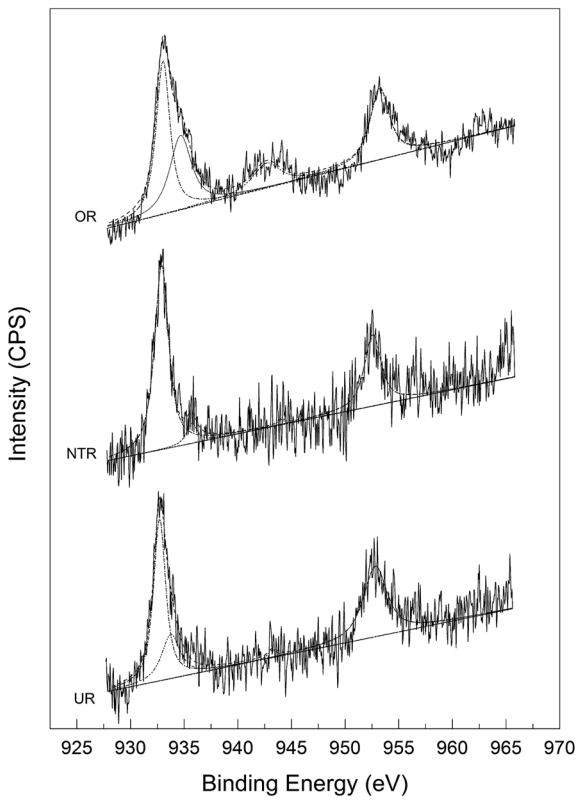

Fig. 9 Cu 2p XPS patterns of OR, NTR, and UR.

As can be seen from the XPS spectra, the primary and shoulder peaks appear at binding energies (B.E.) of around 933 and 943 eV, respectively, for Cu $2p_{3/2}$. As shown in Table 2, the B.E. values of the primary peaks for NTR and UR were slightly lower than that for OR, implying a lower valence of Cu in NTR and UR. This might be attributed to the reduction of CuO by carbon at a high temperature of 400 °C. All of the samples showed a shake-up satellite peak at around 943 eV, which is characteristic of Cu^{2+}. Meanwhile, the weakened satellite peaks for NTR and UR imply decreased amounts of Cu^{2+} and increased amounts of Cu^{+} or Cu^{0} therein. The intensity ratios of the satellite and primary peaks for Cu $2p_{3/2}$ are shown in Table 2. This ratio is about 0.55 for standard CuO and 0 for a Cu^{0} phase.[36] As can be seen in Table 2, NTR showed the lowest valence of Cu, UR showed a slightly higher valence, and OR showed the highest valence.

In addition to the XPS results, the above samples were also analyzed by XRD. As is evident from Fig. 10, CuO peaks were only seen for OR; they were no longer seen for NTR due to complete conversion to Cu_2O and Cu. Supposedly, at a high temperature of 400 °C under nitrogen, the CuO component in the OR sample was successively reduced by AC to Cu_2O and Cu, such that the amount of Cu became dominant. In contrast, only CuO and Cu_2O were found in UR, and no elemental Cu could be detected. This may be the net result of the oxidation of Cu by N_2O and the reduction of CuO by carbon when NTR was heated to 400 °C in N_2O atmosphere. This phenomenon is consistent with earlier investigations by Carabineiro *et al.*,[37,38] and Zhu *et al.*[19]

Based on our experimental evidence and above analysis, the catalytic mechanism of CuO for the reductive removal of N_2O by AC is assumed to proceed as follows:

$$4CuO + C \rightarrow 2Cu_2O + CO_2 \quad (2)$$

$$2Cu_2O + C \rightarrow 4Cu + CO_2 \quad (3)$$

$$2Cu + N_2O \rightarrow Cu_2O + N_2 \quad (4)$$

$$Cu_2O + N_2O \rightarrow 2CuO + N_2 \quad (5)$$

In this process, CuO is involved in transfer of the O atom from N_2O to carbon, accelerating the overall redox reaction between N_2O and AC. In short, AC in the present process serves

Table 2 Cu 2p high-resolution XPS spectra

Sample	Cu $2p_{3/2}$ mp[a] B.E.	Cu $2p_{3/2}$ sp[b] B.E.	Splitting energy[c] (eV)	I_{sp}/I_{mp}[d]
OR	933.1	942.7	9.6	0.21
NTR	932.9	944.0	11.1	0.03
UR	932.7	943.3	10.6	0.04

[a] "mp" denotes the main peak. [b] "sp" denotes the shake-up satellite peak. [c] "splitting energy" is the energy difference between mp and sp. [d] "I_{sp}/I_{mp}" is the intensity ratio of sp and mp.

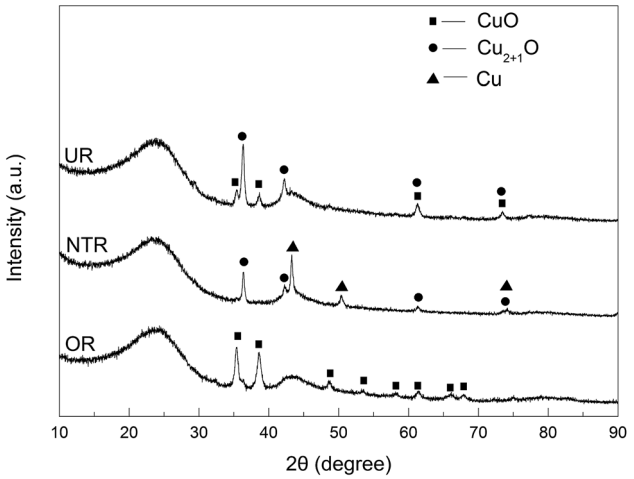

Fig. 10 XRD patterns of loaded ACs in different statuses.

as a consumptive solid reductant for reducing N_2O to nitrogen, while CuO functions as a catalyst for the reaction between N_2O and carbon.

3.5 Applicability and challenge of the present process

Catalytic reduction of N_2O may be achieved at mild conditions by using AC as solid reducing agent and CuO as catalyst. This process is especially suitable for the treatment of tail gas of the adipic acid production process with high concentration of N_2O, and is advantageous due to its safety, ease of control, low operating temperature (300–400 °C), and lower cost of AC. And even the industrial waste AC may be also applicable, which further reduces the raw material cost and makes a resource use of another industrial waste. However, some challenges should be considered and tackled properly, *e.g.* competitive oxidation of O_2 with N_2O and emission of toxic metal oxide nanoparticles from the exhaust gas. In fact, such competitive oxidation is inevitable in all reductive removal processes of N_2O with varying reducing agents, such as H_2, CO, and CH_4. However, the reactivity of N_2O with AC is higher than that of O_2, as manifested by its lower reaction temperature on 0.09Cu-AC-400, *i.e.* 300 °C for N_2O (Fig. 6) and about 375 °C for air (O_2) (Fig. 5). Therefore, the inhibition effect of O_2 for the reduction of N_2O may be quite low at appropriate conditions, for example, the presence of O_2 was found to have no influence on the N_2O-char reactivity at higher temperature.[39,40] In contrast, at lower temperature of 320 °C and lower N_2O content (0.3% N_2O in helium gas), the coexistent 1.5% O_2 may lead to a 20% lowering of reactivity of N_2O on Cu_2O-AC catalyst[25] due to the blocking effect of O_2 for the active sites of AC.[26] As a reducing agent, AC will be oxidized and consumed gradually, and the residue toxic metal oxides may be emitted from the exhaust gas to the atmosphere. However, this problem may be solved through conventional technical approaches. For example, by using a moving-bed reactor, most of the ultrafine metal oxide particles will be retained in the reactor due to the filtering effect of the granular AC catalyst, some of the particles can be collected as sediment in the baffled heat exchanger for cooling the high temperature exhaust gas to ambient temperature, and finally, the ultrafine ashes can be further removed to reach the environmental standard by wet or electrostatic dust collector.

4. Conclusions

N_2O can be completely decomposed by AC at 550 °C through a redox reaction between AC as reductant and N_2O as oxidant. The decomposition reaction is greatly enhanced by some transition metal oxide catalysts, among which CuO has proved to be the best one. Complete removal of N_2O was achieved by 0.09Cu-AC-200 at a much lower temperature of 275 °C. The catalytic mechanism of CuO has been studied by XPS and XRD, which would seem to involve the reduction of CuO to Cu_2O and Cu by AC, and oxidation of Cu to Cu_2O and CuO by N_2O. In this process, CuO is involved in transfer of the O atom from N_2O to carbon, accelerating the overall redox reaction between N_2O and AC.

References

1 M. A. Zamudio, S. Bensaid, D. Fino and N. Russo, *Ind. Eng. Chem. Res.*, 2011, **50**, 2622–2627.
2 N. Li, *Chem. Ind. Eng. Prog.*, 2007, **26**, 1659–1661.
3 Y. Shen, C. Li, Y. Tang and S. Zhu, *RSC Adv.*, 2015, **5**, 13212–13219.
4 S. Kannan, *Appl. Clay Sci.*, 1998, **13**, 347–362.
5 J. K. Lee, Y. J. Kim, H. J. Lee, S. H. Kim, S. J. Cho, I. S. Nam and S. B. Hong, *J. Catal.*, 2011, **284**, 23–33.
6 B. M. Abu-Zied, *Microporous Mesoporous Mater.*, 2011, **139**, 59–66.
7 B. H. Chen, N. Liu, X. Y. Liu, R. D. Zhang, Y. P. Li, Y. X. Li and X. L. Sun, *Catal. Today*, 2011, **175**, 245–255.
8 T. P. Gaidey, *Russ. J. Appl. Chem.*, 2009, **82**, 1689–1705.
9 V. G. Komvokis, M. Marti, A. Delimitis, I. A. Vasalos and K. S. Triantafyllidis, *Appl. Catal., B*, 2011, **103**, 62–71.
10 S. S. Kim, S. J. Lee and S. C. Hong, *Chem. Eng. J.*, 2011, **169**, 173–179.
11 M. Hussain, D. Fino and N. Russo, *J. Hazard. Mater.*, 2012, **211**, 255–265.
12 Q. Zhang, X. Tang, P. Ning, Y. Duan, Z. Song and Y. Shi, *RSC Adv.*, 2015, **5**, 51263–51270.
13 C. Li, Y. Shen, S. Zhu and S. Shen, *RSC Adv.*, 2014, **4**, 29107–29119.
14 T. Xu, C. Wang, X. Wu, B. Zhao, Z. Chen and D. Weng, *RSC Adv.*, 2016, **6**, 97004–97011.
15 M. Mihet, V.-M. Cristea, P.-S. Agachi, A.-M. Cormos and M. D. Lazar, *RSC Adv.*, 2016, **6**, 89259–89273.
16 P. Nematollahia and M. D. Esrafili, *RSC Adv.*, 2016, **6**, 59091–59099.
17 J. Rodriguez-Mirasol, A. C. Ooms, J. R. Pels, F. Kapteijn and J. A. Moulijn, *Combust. Flame*, 1994, **99**, 499–507.
18 Z. H. Zhu and G. Q. Lu, *J. Catal.*, 1999, **187**, 262–274.
19 Z. H. Zhu, G. Q. Lu and R. T. Yang, *J. Catal.*, 2000, **192**, 77–87.
20 F. Gonçalves and J. L. Figueiredo, *Appl. Catal., B*, 2004, **50**, 271–278.

21 F. Gonçalves and J. L. Figueiredo, *Appl. Catal., B*, 2006, **62**, 181–192.
22 Y. Chen, Z. Hu, X. Wang, G. Zhao, Y. Liu and W. Liu, *Acta Phys.-Chim. Sin.*, 2008, **249**, 1589–1596.
23 J. Sun, H. Wang and B. Sun, *Chin. J. Environ. Eng.*, 2011, **5**, 261–266.
24 C. Wang, Y. Liu, X. Zheng, Z. Wen, A. Liu, X. Xu and Z. Hu, *Gongneng Cailiao*, 2010, **9**, 1520–1528.
25 Z. H. Zhu, L. R. Radovic and G. Q. Lu, *Carbon*, 2000, **38**, 451–464.
26 Y. H. Li, G. Q. Lu and V. Rudolph, *Chem. Eng. Sci.*, 1998, **53**, 1–26.
27 S. A. Carabineiro, F. B. Fernandes, A. M. Ramos, J. Vital and I. F. Silva, *Catal. Today*, 2000, **57**, 305–312.
28 A. N. Zhou, X. L. Ma and C. S. Song, *Appl. Catal., B*, 2009, **87**, 190–199.
29 Y. F. Jia and K. M. Thomas, *Langmuir*, 2000, **16**, 1114–1122.
30 B. H. Stuart, *Infrared Spectroscopy: Fundamentals and Applications*, Wiley, 2004.
31 W. N. R. W. Isahak, M. W. M. Hisham and M. A. Yarmo, *J. Chem.*, 2013, **2013**, 1–6.
32 J. Co, P. D. Standards, *Powder Diffraction File*, ASTM, Newtown Square, PA, USA, 2004, pp. 48–1548.
33 L. Chmielarz, M. Rutkowska, P. Kuśtrowski, M. Drozdek, Z. Piwowarska, B. Dudek, R. Dziembaj and M. Michalik, *J. Therm. Anal. Calorim.*, 2011, **105**, 161–170.
34 J. Co, P. D. Standards, *Powder Diffraction File*, ASTM, Newtown Square, PA, USA, 2004, pp. 05–0667.
35 M. C. Campa, V. Indovina and D. Pietrogiacomi, *Appl. Catal., B*, 2012, **111**, 90–95.
36 A. Patel, P. Shukla, T. Rufford, S. Wang, J. Chen, V. Rudolph and Z. H. Zhu, *Appl. Catal., A*, 2011, **409**, 55–65.
37 S. A. Carabineiro, F. B. Fernandes, R. J. C. Silva, J. S. Vital, A. M. Ramos and I. M. Fonseca, *Catal. Today*, 2008, **133**, 441–447.
38 S. A. Carabineiro, F. B. Fernandes, J. S. Vital, A. M. Ramos and I. M. Fonseca, *Appl. Catal., B*, 2005, **59**, 181–186.
39 I. Gulyurtlu, H. Esparteiro and I. Cabrita, *Fuel*, 1994, **73**, 1098–1102.
40 J. Rodriguez-Mirasol, A. C. Ooms, J. R. Pels, F. Kapteijn and J. A. Moulijn, *Combust. Flame*, 1994, **99**, 499–507.